Realization of Su-Schrieffer-Heeger states based on metamaterials of magnetic solitons

Gyungchoon Go,[1,*] Ik-Sun Hong,[2] Seo-Won Lee,[1] Se Kwon Kim,[3] and Kyung-Jin Lee[1,2]
[1]*Department of Materials Science and Engineering, Korea University, Seoul 02841, Korea*
[2]*KU-KIST Graduate School of Converging Science and Technology, Korea University, Seoul 02841, Korea*
[3]*Department of Physics and Astronomy, University of Missouri, Columbia, Missouri 65211, USA*

(Received 10 October 2019; revised manuscript received 23 March 2020; accepted 1 April 2020; published 21 April 2020)

We theoretically investigate coupled gyration modes of magnetic solitons whose distances to the nearest neighbors are staggered. In a one-dimensional bipartite lattice, we analytically and numerically find that there is a midgap gyration mode bounded at the domain wall connecting topologically distinct two phases which is analogous to the Su-Schrieffer-Heeger model. As a technological application, we show that a one-dimensional domain-wall string in a two-dimensional soliton lattice can serve as a waveguide of magnetic excitations, which offers functionalities of a signal localization and selective propagation of the frequency modes. Our result offers an alternative way to control the magnetic excitation modes by using a magnetic metamaterial for future spintronic devices.

DOI: 10.1103/PhysRevB.101.134423

I. INTRODUCTION

Topological properties embedded in band structures are one of the central themes in modern condensed-matter physics. In two-dimensional (2D) electron systems, representative examples supporting topologically protected edge states [1] are the Haldane model [2] and the Kane-Mele model [3], which exhibit the quantum Hall and quantum spin Hall phases, respectively. A classical example in one-dimensional (1D) topological systems is the Su-Schrieffer-Heeger (SSH) model supporting a midgap bound state with fermion number 1/2 [4,5]. Inspired by the topological effects in electronic systems, numerous studies have been devoted to investigating topological properties in bosonic systems such as magnons [6–8], phonons [9,10], and their hybridized states [11–14].

Such topological effects of band structures can also be realized in artificially structured composites, called metamaterials, whose functionalities arise as the collective dynamics of local resonators [15]. Analogs of topologically protected edge states in 2D systems have been proposed and experimentally observed in acoustic [15,16], optical [17–21], magnetic [22–24], mechanical [25,26], and electric circuit [27–29] systems. Moreover, the 1D SSH model has been realized in optical waveguides [30], electric circuits [31,32], and magnetic spheres [33]. An intriguing feature of the metamaterials is that the band structures and their topological properties can be manipulated by changing the crystal parameters. This tunability of metamaterials is of crucial importance for widespread applications of topological properties in, for instance, reconfigurable logic devices [15,19].

Magnetic solitons such as magnetic vortices and skyrmions are resonators whose dynamics exhibit gyroscopic motion [34–36]. Theoretical [37–39] and experimental [40–42] results on the dynamics of coupled gyration modes of the magnetic solitons provide a potential application for a different type of information device [39]. Moreover, internal degrees of freedom of magnetic solitons such as polarity and chirality can offer efficient control of the functionalities of soliton-based metamaterials [43]. One of us has shown that the collective excitation of the magnetic solitons supports a chiral edge mode in a honeycomb lattice [23], which was later confirmed by micromagnetic simulation [24]. Recently, the topological corner states have been realized in breathing kagome [44] and honeycomb lattice [45]. However, the SSH state in the 1D system has not been realized for collective gyration modes of magnetic solitons.

In this paper, we first study a metamaterial composed of the magnetic soliton disks structured in a one-dimensional bipartite chain. By using both analytic calculation and micromagnetic simulation, we show the existence of a midgap state bounded at a domain wall connecting topologically distinct two configurations, which is analogous to the electronic SSH model. Then we derive a 2D extension of our 1D magnetic SSH model, which is shown to be able to support a magnetic waveguide with selective propagation of frequency modes.

II. REALIZATION OF THE SSH MODEL WITH AN ARRAY OF SOLITON DISKS

We consider a quasi-one-dimensional array of nanodisks containing magnetic vortices or skyrmions. In general, the steady-state motion of topological solitons can be described by the dynamics of the center-of-mass position $\mathbf{R}(t)$ and $\mathbf{m} = \mathbf{m}[\mathbf{r} - \mathbf{R}(t)]$, where $\mathbf{m}$ is a unit vector along the direction of local magnetization. The dissipationless magnetization dynamics of the coupled vortices/skyrmions is described by Thiele's equation [46]:

$$G\hat{\mathbf{z}} \times \frac{d\mathbf{U}_j}{dt} + \mathbf{F}_j = 0, \tag{1}$$

*gyungchoon@gmail.com

where $\mathbf{U}_j = \mathbf{R}_j - \mathbf{R}_j^0$ is the displacement of the soliton from the equilibrium position $\mathbf{R}_j^0$, $G = -4\pi M_s t_D Q/\gamma$ is the gyrotropic coefficient, M_s is the saturation magnetization, t_D is the thickness of the disk, and γ is the gyromagnetic ratio. Here, $Q = \frac{1}{4\pi}\int dxdy\mathbf{m}\cdot(\partial_x\mathbf{m}\times\partial_y\mathbf{m})$ is the topological charge which characterizes the topological solitons. The topological charge of the magnetic vortices and skyrmions are $Q = \pm 1/2$ and ± 1, respectively. $\mathbf{F}_j = -\partial W/\partial \mathbf{U}_j$ is the conservative force from the potential energy

$$W = \sum_j \frac{K}{2}\mathbf{U}_j^2 + \sum_{j\neq k}\frac{U_{jk}}{2}, \tag{2}$$

where $K > 0$ is the spring constant and $\mathbf{U}_j \equiv (u_j, v_j)$ is the displacement vector. Here, U_{jk} is the interaction energy between two solitons:

$$U_{jk}(d_{jk}) = I_x(d_{jk})u_j u_k - I_y(d_{jk})v_j v_k, \tag{3}$$

where $d_{jk}(= |\mathbf{R}_j^0 - \mathbf{R}_k^0|)$ is the distance between centers of two neighboring disks, and $I_x(d_{jk})$ and $I_y(d_{jk})$ are interaction parameters between two disks. This system of coupled magnetic solitons has been studied both theoretically and experimentally [37,38,41,42]. In particular, the values of the parameters in Eqs. (2) and (3) have been experimentally measured and theoretically calculated for certain sizes of soliton disks.

Let us first consider the situation where the nearest-neighbor disk pairs are separated by a uniform distance. Using the complex variable $\psi_j \equiv u_j + iv_j$, we write Eq. (1) in a simplified form [23,24]:

$$i\dot{\psi}_j = \omega_K\psi_j + \sum_{k\in\langle j\rangle}(\zeta\psi_k + \xi\psi_k^*), \tag{4}$$

where $\omega_K = K/G$ is the gyration frequency of an isolated soliton and $\zeta = (I_x - I_y)/G$ and $\xi = (I_x + I_y)/G$ are the reparametrized interactions. In order to eliminate ψ_k^*, we expand the complex variable as

$$\psi_j = \chi_j\exp(-i\omega_0 t) + \eta_j\exp(i\omega_0 t), \tag{5}$$

where $\chi_j(\eta_j)$ is a counterclockwise (clockwise) gyration amplitude. Substituting Eq. (5) into Eq. (4) and applying $|\chi_j| \gg |\eta_j|$ ($|\chi_j| \ll |\eta_j|$) for counterclockwise (clockwise) soliton gyrations, we have

$$i\dot{\psi}_j = \left(\omega_K - \frac{\xi^2}{\omega_K}\right)\psi_j + \zeta\sum_{k\in\langle j\rangle}\psi_k - \frac{\xi^2}{2\omega_K}\sum_{l\in\langle\langle j\rangle\rangle}\psi_l, \tag{6}$$

where $\langle\langle j\rangle\rangle$ represents second-neighbor sites of j. The right-hand side of Eq. (6) contains zeroth-order (ω_K), first-order (ζ), and second-order (ξ^2) terms of the interdisk interactions. For 1D chain systems, we have

$$i\dot{\psi}_j = \left(\omega_K - \frac{\xi^2}{\omega_K}\right)\psi_j + \zeta(\psi_{j+1} + \psi_{j-1}) - \frac{\xi^2}{2\omega_K}(\psi_{j+2} + \psi_{j-2}). \tag{7}$$

Taking the Fourier transformation, we obtain an eigenvalue equation, $i\dot{\Psi}(k_x, t) = H_k\Psi(k_x, t)$ with a momentum space Hamiltonian

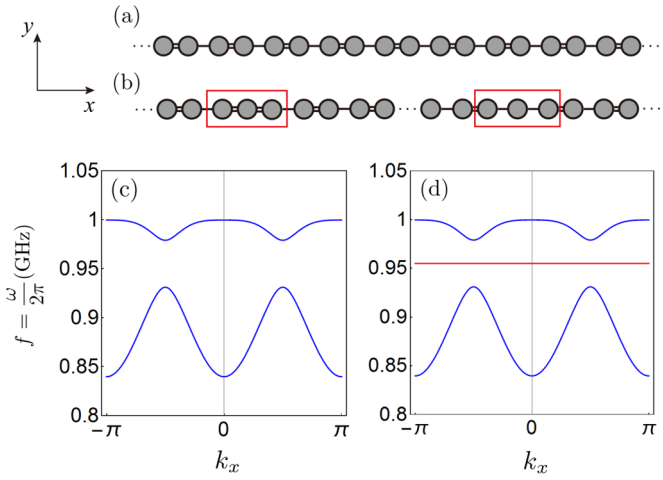

FIG. 1. A schematic illustration of the staggered 1D chain of magnetic nanodisks without the domain-wall defect (a), and with a pair of domain-wall and anti-domain-wall defects (b). A single (double) bond represents the longer (shorter) interdisk distance. Band structure of the system without the domain-wall defect (c), and with a pair of domain-wall and anti-domain-wall defects (d). A pair of states at $\omega = \omega_K$ is induced by the defects (red).

$$H_k = \omega_K + 2\zeta\cos k_x - \frac{2\xi^2}{\omega_K}\cos^2 k_x, \tag{8}$$

describing a single-band Hamiltonian of magnetic excitations.

Now, let us consider a staggered 1D chain of magnetic nanodisks [Fig. 1(a)] with periodic boundary condition which mimics the SSH system [4]. Because of the staggered lattice structure, the interdisk interactions (ζ and ξ) are divided into two different types:

$$\zeta \to \begin{cases}\zeta(1+\Delta)\\ \zeta(1-\Delta)\end{cases}, \qquad \xi \to \begin{cases}\xi(1+\Delta')\\ \xi(1-\Delta')\end{cases}. \tag{9}$$

Here, Δ and Δ', which can be either positive or negative, represent the staggeredness of the SSH system. By substituting Eq. (9) into Eq. (6) and introducing sublattice indices A and B, we have

$$\begin{aligned} i\dot{\psi}_{2m}^A = &\left(\omega_K - \frac{\xi^2(1+\Delta'^2)}{\omega_K}\right)\psi_{2m}^A \\ &+ \zeta(1+\Delta)\psi_{2m+1}^B + \zeta(1-\Delta)\psi_{2m-1}^B \\ &- \frac{\xi^2(1-\Delta'^2)}{2\omega_K}\left(\psi_{2m-2}^A + \psi_{2m+2}^A\right), \end{aligned} \tag{10}$$

$$\begin{aligned} i\dot{\psi}_{2m+1}^B = &\left(\omega_K - \frac{\xi^2(1+\Delta'^2)}{\omega_K}\right)\psi_{2m+1}^B \\ &+ \zeta(1-\Delta)\psi_{2m+2}^A + \zeta(1+\Delta)\psi_{2m}^A \\ &- \frac{\xi^2(1-\Delta'^2)}{2\omega_K}\left(\psi_{2m-1}^B + \psi_{2m+3}^B\right). \end{aligned} \tag{11}$$

We note that $\xi^2\Delta'^2$ terms, which are induced from the staggeredness of ξ, appear in the identity matrix part of the momentum space Hamiltonian. Because these terms cannot

change the topology of the Hamiltonian and are negligible in the small Δ' limit, we discard $\xi^2\Delta'^2$ terms in this paper. Taking the Fourier transformation, we obtain

$$H_k = \begin{pmatrix} \omega_K - \frac{2\xi^2}{\omega_K}\cos^2 k_x & 2\zeta(\cos k_x - i\Delta \sin k_x) \\ 2\zeta(\cos k_x + i\Delta \sin k_x) & \omega_K - \frac{2\xi^2}{\omega_K}\cos^2 k_x \end{pmatrix} = \left(\omega_K - \frac{2\xi^2}{\omega_K}\cos^2 k_x\right) I_{2\times 2} + \mathbf{n}(k_x)\cdot\boldsymbol{\sigma}, \quad (12)$$

where the basis of the Hamiltonian is $\Psi(k_x) = (\psi^A(k_x), \psi^B(k_x))^T$ and $\boldsymbol{\sigma} = (\sigma_x, \sigma_y)$ are the Pauli matrices. The eigenvalues of Eq. (12) are given by

$$\omega_\pm = \omega_K - \frac{2\xi^2}{\omega_K}\cos^2 k_x \pm 2\zeta\sqrt{\cos^2 k_x + \Delta^2 \sin^2 k_x}\,. \quad (13)$$

In Fig. 1(c), we show the dispersion relation of Eq. (13). For calculation, we take the model parameters $\omega_K/2\pi = 0.955\,\mathrm{GHz}$, $\zeta/2\pi = -0.04\,\mathrm{GHz}$, $\xi/2\pi = 0.13\,\mathrm{GHz}$, and $\Delta = 0.3$ in accordance with micromagnetic simulation results in next section. The staggeredness Δ induces a finite gap. We note that the particle-hole symmetry is broken because of the momentum dependent diagonal component in Eq. (12) from the second-order interactions ($-\frac{2\xi^2}{\omega_K}\cos^2 k_x I_{2\times 2}$). The second-order interaction term can be treated as a smooth perturbation of the Hamiltonian and does not change the topological character of the system. The topological number of the Hamiltonian (12) is the winding number of the two-component unit vector $\hat{\mathbf{n}}(k_x) = \mathbf{n}(k_x)/|\mathbf{n}(k_x)| \equiv (\cos\theta_k, \sin\theta_k)$ which is expressed by the integral [47–49]

$$N = \frac{1}{2\pi}\int_{\mathrm{BZ}} dk_x \left(\frac{d\theta_k}{dk_x}\right) = \mathrm{sgn}(\Delta), \quad (14)$$

where $\theta_k = \tan^{-1}(n_y/n_x) = \tan^{-1}(\Delta \tan k_x)$ is a polar angle of the unit vector in momentum space. The winding number is corresponding to the homotopy map $\pi_1(S^1) = \mathbb{Z}$. Equation (14) implies that there are two topologically distinct phases which are represented by the sign of Δ.

Expanding Eq. (12) around $k_x = \pi/2$, which minimizes the band gap, we obtain an effective Dirac Hamiltonian

$$H_k = \begin{pmatrix} \omega_K & -2\zeta\left[\left(k_x - \frac{\pi}{2}\right) + i\Delta\right] \\ -2\zeta\left[\left(k_x - \frac{\pi}{2}\right) - i\Delta\right] & \omega_K \end{pmatrix}. \quad (15)$$

Diagonalizing Eq. (15), we obtain the eigenfrequencies with a band gap Δ,

$$\omega_\pm = \omega_K \pm 2\zeta\sqrt{\left(k_x - \frac{\pi}{2}\right)^2 + \Delta^2}. \quad (16)$$

Because a topological bound state exists at the interface between the two topologically distinct phases, we consider a situation where the staggeredness Δ is reversed its sign at $x = 0$: $\Delta(x) = \Delta_0\mathrm{sgn}(x)$. In this case, a midgap bound state appears at $\omega = \omega_K$, without changing the bulk dispersions of upper and lower bands [see Fig. 1(d)]. From Eq. (15), we read that the midgap bound state satisfies

$$\begin{pmatrix} 0 & i\partial_x - i\Delta(x) \\ i\partial_x + i\Delta(x) & 0 \end{pmatrix}\Psi_{\mathrm{bound}} = 0, \quad (17)$$

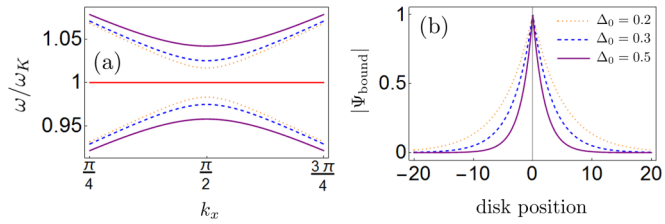

FIG. 2. Band structures of the Dirac Hamiltonian (a) and localization of the bound state (b) for $\Delta_0 = 0.2$ (dotted), $\Delta_0 = 0.3$ (dashed), and $\Delta_0 = 0.5$ (solid).

which results in

$$\Psi_{\mathrm{bound}}(x) \sim \begin{pmatrix} 0 \\ e^{-\Delta_0|x|} \end{pmatrix} \quad (\Delta_0 > 0),$$
$$\Psi_{\mathrm{bound}}(x) \sim \begin{pmatrix} e^{\Delta_0|x|} \\ 0 \end{pmatrix} \quad (\Delta_0 < 0). \quad (18)$$

Equation (18) shows that the bound state is exponentially localized at the domain wall. This is a magnetic analog of the SSH system which possesses a soliton with half-electric charge [4]. Creation of the bound state is compensated by one-half of a state missing from the two bulk bands corresponding to $\omega = \omega_\pm$. In Fig. 2, we show the band structures of the effective Dirac Hamiltonian in Eq. (15) and localization of the bound state for different values of Δ_0.

III. MICROMAGNETIC SIMULATION

We perform micromagnetic simulations to visualize the collective dynamics of the magnetic vortex lattice. Here, we use following parameters of typical permalloy [37]: the saturation magnetization $M_s = 800\ \mathrm{erg/cm^3}$, the exchange stiffness $A = 1.3\times 10^{-6}$ erg/cm. In order to obtain the clear fast Fourier transform (FFT) image, we choose a small Gilbert damping constant $\alpha = 0.001$. The diameter and thickness of magnetic nanodisk are chosen to be 80 and 20 nm, respectively. The unit-cell size is chosen to be $4\times 4\times 20\ \mathrm{nm^3}$.

We consider a 1D bipartite chain of 40 identical magnetic nanodisks with a periodic boundary condition as shown in Fig. 3(a). Each disk has a magnetic vortex with the same polarity ($p = 1$) and chirality ($C = -1$) [see Fig. 3(b)]. We simulate the collective dynamics of the vortex gyration in the bipartite lattice with a domain wall (11th disk) and an anti-domain wall (31st disk) which are separated by 20 disks. To obtain the dispersion relation of collective vortex gyration modes, we apply a sinc function of external magnetic field,

$$\mathbf{H}(t) = H_0 \sin[2\pi f(t - t_0)]/[2\pi f(t - t_0)]\hat{\mathbf{x}}, \quad (19)$$

on one of the disks with $H_0 = 10\,\mathrm{mT}$, $f = 20\,\mathrm{GHz}$, and $t_0 = 1\,\mathrm{ns}$.

Then, we obtain the dispersion relation from the fast Fourier transform (FFT) of the temporal oscillations of x component of the vortex core position. Figure 3(d) shows the resonant spectrum of a vortex gyration mode in an isolated magnetic nanodisk. We find that the single vortex

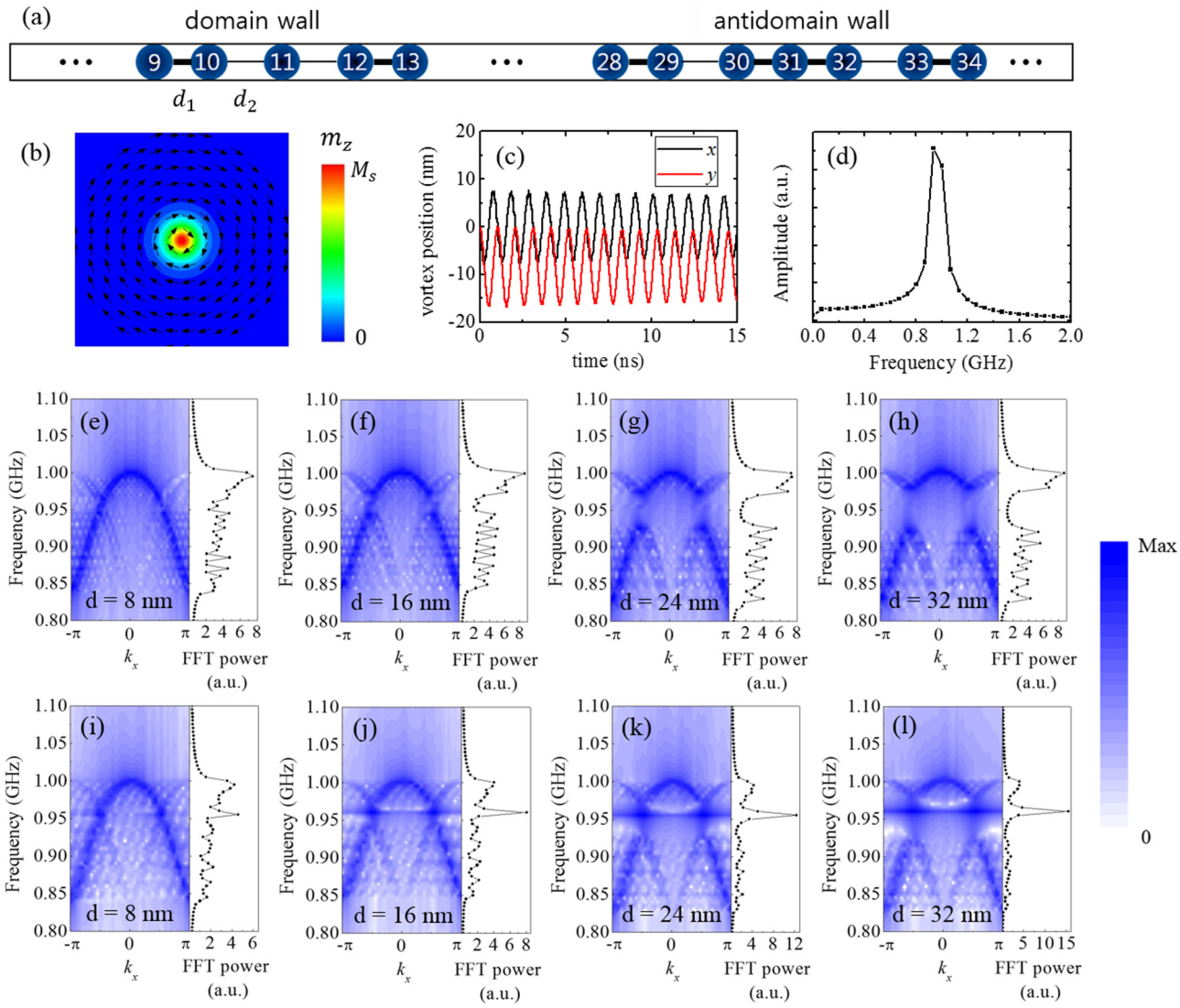

FIG. 3. (a) Illustration of the 1D bipartite lattice of magnetic nanodisk with a domain wall (11th disk) and an antidomain wall (31st disk) profile. (b) A magnetic nanodisk containing a single vortex. (c) Vortex core dynamics in an isolated magnetic nanodisk. (d) Resonant spectrum of single vortex gyration in an isolated magnetic nanodisk. Dispersion relation of collective vortex gyration in the bipartite lattice when the external field is far away from the domain-wall position (21st disk) with interdisk distance $[d_1, d_2]$ of (e) [16 nm, 24 nm], (f) [12 nm, 28 nm], (g) [8 nm, 32 nm], and (h) [4 nm, 36 nm], and when the external field is on the domain-wall position (11th disk) with interdisk distance of (i) [16 nm, 24 nm], (j) [12 nm, 28 nm], (k) [8 nm, 32 nm], and (l) [4 nm, 36 nm].

gyration mode has a peak at $f_0 = \omega_K/2\pi = 0.955\,\mathrm{GHz}$. Figures 3(e)–3(h) show the dispersion relation of the bipartite chain when the external field is located far away from the domain-wall position (21st disk). As the difference of interdisk distance ($d = d_2 - d_1$) increases, a more distinct band splitting (into upper and lower bands) is observed. Note that the in-gap mode between the upper and lower bands has not been excited in this case, because it is localized on the defect position and thus far away from the external-field position. When the external field locates on the domain-wall position (11th disk), we find that a midgap mode is excited near f_0 without significant change of the bulk dispersion [Figs. 3(i)–3(l)]. The simulation results coincide with the analytic results in Sec. II with appropriate model parameters [see Figs. 1(c) and 1(d)].

IV. 2D MAGNETIC WAVEGUIDE

Now let us consider a 2D extension of our 1D magnetic SSH model, which will be shown to support a magnetic waveguide of excitations below. The schematic illustration of the 2D lattice is shown in Fig. 4(a). The 2D extended model includes additional interactions proportional to ζ^y, $\xi_y^2/2\omega_K$, and $\xi_{xy}^2(1 \pm \bar{\Delta})/2\omega_K$ [see Fig. 4(b)]. We note that $\bar{\Delta}$ represents the staggeredness of the second-order interactions, and its sign is reversed at the defect position. In momentum space representation, we have an effective Hamiltonian (see the Appendix)

$$H^{2D}(k_x, k_y) = \begin{pmatrix} H^{AA} & H^{AB} \\ (H^{AB})^* & H^{BB} \end{pmatrix}, \tag{20}$$

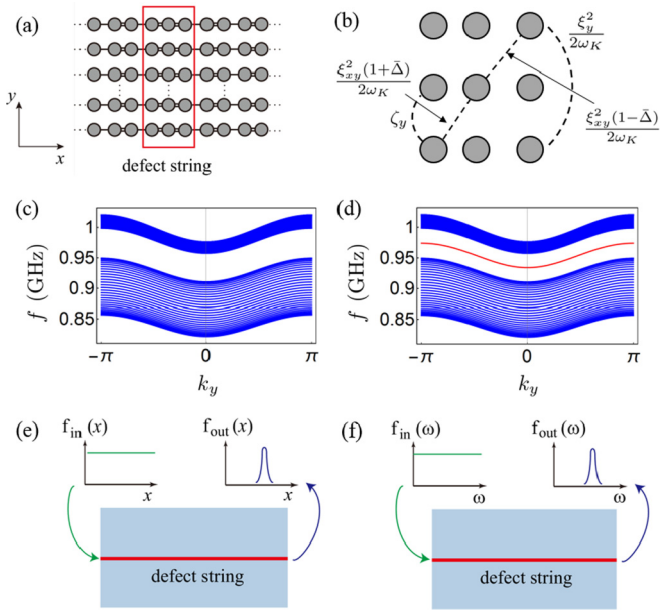

FIG. 4. (a) A schematic illustration a two-dimensional extension of the 1D magnetic SSH model. (b) Additional interactions of the 2D tight-binding model. Bulk and bound-state dispersions of the 2D model without the domain-wall defect (c) and with the domain-wall defect (d). For calculation, we take the model parameters $\omega_K/2\pi = 0.955\,\mathrm{GHz}$ $\zeta/2\pi = -0.04\,\mathrm{GHz}$, $\xi/2\pi = 0.13\,\mathrm{GHz}$, $\Delta = 0.3$, $\zeta_y = \zeta/4$, $\xi_{xy} = \xi/4$, $\xi_y = \xi/6$, and $\bar{\Delta} = \Delta$. (e) Magnetic wave propagation in the magnetic waveguide supporting signal localization. (f) Magnetic wave propagation in the magnetic waveguide supporting selective propagation of frequency.

where

$$H^{AA} = \omega_0^{2D} - \frac{2\xi^2}{\omega_K}\cos^2 k_x = H^{BB}, \tag{21}$$

$$H^{AB} = 2\zeta(\cos k_x - i\Delta \sin k_x) + \frac{2\xi_{xy}^2}{\omega_0}\cos k_y(\cos k_x - i\bar{\Delta}\sin k_x), \tag{22}$$

and $\omega_0^{2D}(k_y) = \omega_K - \frac{2\xi_y^2}{\omega_K}\cos^2 k_y + 2\zeta_y \cos k_y$. The additional interactions yield the additional dispersion along k_y direction. The resultant 2D band dispersions without and with the (stringlike) domain-wall defect are shown in Figs. 4(c) and 4(d), respectively. In the 2D lattice, the pointlike defect in the 1D model is extended in the y direction and forms a domain-wall string. In the presence of the domain-wall defect, we find that the bound state with a frequency $\omega_0^{2D}(k_y)$ is localized on the defect position (see the Appendix).

In this 2D soliton lattice model, the topological midgap bound states are localized at the defect position and spatially connected in the y direction. Therefore, magnetic excitations on the bound state propagate well along the defect string with a small spread in the transverse (x) direction. This propagation characteristic realizes a magnetic waveguide by using magnetic solitons with signal localization and selective propagation of frequency modes. Figures 4(e) and 4(f) show the schematic illustration of two functionalities of the magnetic soliton waveguide. In Fig. 4(e), the incoming wave packet is a plane wave (i.e., uniform along the x direction) and has a frequency corresponding to the bound state. Because this frequency mode can only propagate through the defect string, the outgoing wave packet is localized on the defect site. In Fig. 4(f), the incoming wave packet on the defect site is a white signal having equal intensities for all frequencies. However, most frequency modes on the defect site cannot propagate in the y direction, except for the bound state. As a result, the outgoing wave packet on the defect site has a peak at a frequency corresponding to the bound state. Unfortunately, in our magnetic waveguide, we cannot obtain a single frequency outgoing wave packet because the group velocity along the bound state (v_y) is very small if the bandwidth of the bound state is too narrow. For a waveguide with finite group velocity, we need some intermediate values of y-directional hopping parameters. In Figs. 4(c) and 4(d), we choose a set of parameters which results in $\overline{|v_y|}/\overline{|v_x^{\mathrm{upper}}|} \approx 1$ and $\overline{|v_y|}/\overline{|v_x^{\mathrm{lower}}|} \approx 0.4$, where $\overline{|v_x^{\mathrm{upper}}|}$ and $\overline{|v_x^{\mathrm{lower}}|}$ are the averaged absolute value of group velocities (along the x direction) of the upper and lower band over the first Brillouin zone, respectively.

Note that our 2D magnetic waveguide does not show the topologically protected (back-scattering free) transport. Any disorders or defects in our 2D waveguide give rise to back-scattering for transport along the waveguide. However, the existence of the waveguide with frequencies separated from the bulk bands is topological in a sense that the waveguide is composed of topological modes in each SSH chain.

We note that the frequency of the bound state is mainly determined by the gyrotropic frequency of a single magnetic soliton, which is tunable by external perturbations. For example, in the presence of an effective magnetic field H_{eff} perpendicular to the disk plane, the gyrotropic frequency can be described as [50,51]

$$\omega \simeq \frac{K}{G}(1 + kH_{\mathrm{eff}}), \tag{23}$$

where k is a proportionality constant. This suggests that the waveguide property can be manipulated by the external magnetic field or voltage-induced magnetic anisotropy change [52].

V. CONCLUSION

To summarize, we have studied collective dynamics in a one-dimensional bipartite chain of the magnetic vortices or skyrmions. In our magnetic system, the domain-wall-like defects are produced by changing the interdisk distances. We have found that the defects induce the midgap states which are confined at the defect position. We also provide the micromagnetic simulation results supporting the analytic results. Our finding on the 1D model is analogous to that of the SSH model in the electron system. In contrast to the electronic SSH model, in which it is hard to manipulate the domain-wall profiles of atomic arrangement, the topological manipulation is feasible in our magnetic SSH model. As a technological application, we propose a two-dimensional extension of our 1D model, which supports a magnetic waveguide of magnetic excitations. The magnetic waveguide provides not only a signal localization but also selective propagation of the frequency

modes. Our work suggests that a spintronics device based on magnetic metamaterials can offer a way for precise control of the the oscillation of magnetic soliton lattice.

ACKNOWLEDGMENTS

G.G. was supported by the National Research Foundation of Korea (NRF) (Grant No. NRF-2019R1I1A1A01063594). S.K.K. was supported by a Young Investigator Grant (YIG) from Korean-American Scientists and Engineers Association (KSEA) and Research Council Grant No. URC-19-090 of the University of Missouri. K.-J.L. acknowledges support by the NRF (Grant No. NRF-2020R1A2C3013302).

G.G. and I.-S.H. contributed equally to this work.

APPENDIX: COMPUTATIONAL DETAILS OF THE 2D MODEL

Here, we derive the effective Hamiltonian of the 2D extension of our 1D magnetic SSH model. The lattice structure of our 2D model is shown in Fig. 4(a) and the second-order interactions are shown in Fig. 4(b). By using Eq. (6) of Ref. [23], we write

$$\begin{aligned} i\dot{\psi}^A_{2m} =& \left(\omega_K - \frac{\xi^2+{\xi_y}^2}{\omega_K}\right)\psi^A_{2m} + \zeta(1+\Delta)\psi^B_{2m+\mathbf{x}} + \zeta(1-\Delta)\psi^B_{2m-\mathbf{x}} + \zeta_y\left(\psi^A_{2m+\mathbf{y}} + \psi^A_{2m-\mathbf{y}}\right) \\ &- \frac{\xi^2}{2\omega_K}\left(\psi^A_{2m+2\mathbf{x}} + \psi^A_{2m-2\mathbf{x}}\right) - \frac{\xi_y^2}{2\omega_K}\left(\psi^A_{2m+2\mathbf{y}} + \psi^A_{2m-2\mathbf{y}}\right) \\ &+ \frac{\xi_{xy}^2(1+\bar{\Delta})}{2\omega_K}\left(\psi^B_{2m+\mathbf{x}+\mathbf{y}} + \psi^B_{2m+\mathbf{x}-\mathbf{y}}\right) + \frac{\xi_{xy}^2(1-\bar{\Delta})}{2\omega_K}\left(\psi^B_{2m-\mathbf{x}+\mathbf{y}} + \psi^B_{2m-\mathbf{x}-\mathbf{y}}\right), \end{aligned} \tag{A1}$$

$$\begin{aligned} i\dot{\psi}^B_{2m+\mathbf{x}} =& \left(\omega_K - \frac{\xi^2+{\xi_y}^2}{\omega_K}\right)\psi^B_{2m+\mathbf{x}} + \zeta(1-\Delta)\psi^A_{2m+2\mathbf{x}} + \zeta(1+\Delta)\psi^A_{2m} + \zeta_y\left(\psi^B_{2m+\mathbf{x}+\mathbf{y}} + \psi^B_{2m+\mathbf{x}-\mathbf{y}}\right) \\ &- \frac{\xi^2}{2\omega_K}\left(\psi^B_{2m+3\mathbf{x}} + \psi^B_{2m-\mathbf{x}}\right) - \frac{\xi_y^2}{2\omega_K}\left(\psi^B_{2m+\mathbf{x}+2\mathbf{y}} + \psi^B_{2m+\mathbf{x}-2\mathbf{y}}\right) \\ &+ \frac{\xi_{xy}^2(1-\bar{\Delta})}{2\omega_K}\left(\psi^A_{2m+2\mathbf{x}+\mathbf{y}} + \psi^A_{2m+2\mathbf{x}-\mathbf{y}}\right) + \frac{\xi_{xy}^2(1+\bar{\Delta})}{2\omega_K}\left(\psi^A_{2m+\mathbf{y}} + \psi^A_{2m-\mathbf{y}}\right). \end{aligned} \tag{A2}$$

In Eqs. (A1) and (A2), we neglect $\xi^2\Delta'^2/\omega_K$ terms which are induced from the staggeredness of ξ. Taking the Fourier transformation, we obtain a momentum space Hamiltonian

$$H^{2D}(k_x, k_y) = \begin{pmatrix} H^{AA} & H^{AB} \\ H^{BA} & H^{BB} \end{pmatrix}, \tag{A3}$$

where

$$H^{AA} = \omega_K - \frac{2\xi^2}{\omega_K}\cos^2 k_x - \frac{2\xi_y^2}{\omega_K}\cos^2 k_y + 2\zeta_y \cos k_y = H^{BB}, \tag{A4}$$

$$H^{AB} = 2\zeta(\cos k_x - i\Delta \sin k_x) + \frac{2\xi_{xy}^2}{\omega_0}\cos k_y(\cos k_x - i\bar{\Delta}\sin k_x) = (H^{BA})^*. \tag{A5}$$

In order to obtain the bound-state solution, we expand the Hamiltonian around $k_x = \pi/2$ and replace $k_x - \pi/2$ to $-i\partial_x$. Then we have

$$H^{AA} = \omega_0^{2D}(k_y) = H^{BB}, \tag{A6}$$

$$H^{AB} = 2\zeta(i\partial_x - i\Delta) + \frac{2\xi_{xy}^2}{\omega_0}\cos k_y(i\partial_x - i\bar{\Delta}) = 2\zeta[1+\alpha(k_y)]i\partial_x - 2i\zeta\Delta[1+\beta(k_y)] = (H^{BA})^*, \tag{A7}$$

where $\omega_0^{2D}(k_y) = \omega_K - \frac{2\xi_y^2}{\omega_K}\cos^2 k_y + 2\zeta_y \cos k_y$, $\alpha(k_y) = \frac{\xi_{xy}^2}{\zeta}\omega_K \cos k_y$, $\beta(k_y) = \frac{\bar{\Delta}}{\Delta}\alpha(k_y)$. In the presence of the domain-wall defect, i.e., $\Delta(x) = \Delta_0 \mathrm{sgn}(x)$ and $\bar{\Delta}(x) = \bar{\Delta}_0 \mathrm{sgn}(x)$, by solving the Schrödinger equation

$$H^{2D}(x, k_y)\Psi_{\mathrm{bound}}(x, k_y) = \omega_0^{2D}(k_y)\Psi_{\mathrm{bound}}(x, k_y), \tag{A8}$$

we obtain the bound-state solution which is confined at the defect position:

$$\begin{aligned} \Psi_{\mathrm{bound}}(x, k_y) &\sim \begin{pmatrix} 0 \\ e^{-\rho(k_y)\Delta_0|x|} \end{pmatrix} \quad (\Delta_0 > 0), \\ \Psi_{\mathrm{bound}}(x, k_y) &\sim \begin{pmatrix} e^{-\rho(k_y)\Delta_0|x|} \\ 0 \end{pmatrix} \quad (\Delta_0 < 0), \end{aligned} \tag{A9}$$

where $\rho(k_y) = \frac{1+\beta(k_y)}{1+\alpha(k_y)}$.

[1] Y. Hatsugai, Phys. Rev. Lett. **71**, 3697 (1993).
[2] F. D. M. Haldane, Phys. Rev. Lett. **61**, 2015 (1988).
[3] C. L. Kane and E. J. Mele, Phys. Rev. Lett. **95**, 146802 (2005).
[4] W. P. Su, J. R. Schrieffer, and A. J. Heeger, Phys. Rev. Lett. **42**, 1698 (1979); Phys. Rev. B **22**, 2099 (1980); M. J. Rice and E. J. Mele, Phys. Rev. Lett. **49**, 1455 (1982).
[5] R. Jackiw and C. Rebbi, Phys. Rev. D **13**, 3398 (1976).
[6] H. Katsura, N. Nagaosa, and P. A. Lee, Phys. Rev. Lett. **104**, 066403 (2010).
[7] Y. Onose, T. Ideue, H. Katsura, Y. Shiomi, N. Nagaosa, and Y. Tokura, Science **329**, 297 (2010).
[8] R. Matsumoto and S. Murakami, Phys. Rev. Lett. **106**, 197202 (2011).
[9] L. Zhang, J. Ren, J.-S. Wang, and B. Li, Phys. Rev. Lett. **105**, 225901 (2010).
[10] L. Zhang and Q. Niu, Phys. Rev. Lett. **115**, 115502 (2015).
[11] R. Takahashi and N. Nagaosa, Phys. Rev. Lett. **117**, 217205 (2016).
[12] X. Zhang, Y. Zhang, S. Okamoto, and D. Xiao, Phys. Rev. Lett. **123**, 167202 (2019).
[13] S. Park and B.-J. Yang, Phys. Rev. B **99**, 174435 (2019).
[14] G. Go, S. K. Kim, and K.-J. Lee, Phys. Rev. Lett. **123**, 237207 (2019).
[15] G. Ma and P. Sheng, Sci. Adv. **2**, e1501595 (2016).
[16] Z. Yang, F. Gao, X. Shi, X. Lin, Z. Gao, Y. Chong, and B. Zhang, Phys. Rev. Lett. **114**, 114301 (2015).
[17] F. D. M. Haldane and S. Raghu, Phys. Rev. Lett. **100**, 013904 (2008).
[18] Z. Wang, Y. Chong, J. D. Joannopoulos, and M. Soljčić, Nature (London) **461**, 772 (2009).
[19] X. Cheng, C. Jouvaud, X. Ni, S. H. Mousavi, A. Z. Genack, and A. B. Khanikaev, Nat. Mater. **15**, 542 (2016).
[20] G. Harari, M. A. Bandres, Y. Lumer, M. C. Rechtsman, Y. D. Chong, M. Khajavikhan, D. N. Christodoulides, and M. Segev, Science **359**, eaar4003 (2018).
[21] M. A. Bandres, S. Wittek, G. Harari, M. Parto, J. Ren, M. Segev, D. N. Christodoulides, and M. Khajavikhan, Science **359**, eaar4005 (2018).
[22] R. Shindou, J.-i. Ohe, R. Matsumoto, S. Murakami, and E. Saitoh, Phys. Rev. B **87**, 174402 (2013); R. Shindou, R. Matsumoto, S. Murakami, and J.-i. Ohe, *ibid.* **87**, 174427 (2013).
[23] S. K. Kim and Y. Tserkovnyak, Phys. Rev. Lett. **119**, 077204 (2017).
[24] Z.-X. Li, C. Wang, Y. Cao, and P. Yan, Phys. Rev. B **98**, 180407(R) (2018).
[25] P. Wang, L. Lu, and K. Bertoldi, Phys. Rev. Lett. **115**, 104302 (2015).
[26] L. M. Nash, D. Kleckner, A. Read, V. Vitelli, A. M. Turner, and W. T. M. Irvine, Proc. Natl. Acad. Sci. USA **112**, 14495 (2015).
[27] V. V. Albert, L. I. Glazman, and L. Jiang, Phys. Rev. Lett. **114**, 173902 (2015).
[28] Y. Li, Y. Sun, W. W. Zhu, Z. W. Guo, J. Jiang, T. Kariyado, H. Chen, and X. Hu, Nat. Commun. **9**, 4598 (2018).
[29] W. Zhu, Y. Long, H. Chen, and J. Ren, Phys. Rev. B **99**, 115410 (2019).
[30] J. M. Zeuner, M. C. Rechtsman, Y. Plotnik, Y. Lumer, S. Nolte, M. S. Rudner, M. Segev, and A. Szameit, Phys. Rev. Lett. **115**, 040402 (2015).
[31] C. H. Lee, S. Imhof, C. Berger, F. Bayer, J. Brehm, L. W. Molenkamp, T. Kiessling, and R. Thomale, Commun. Phys. **1**, 39 (2018).
[32] W. Cai, J. Han, F. Mei, Y. Xu, Y. Ma, X. Li, H. Wang, Y. P. Song, Z.-Y. Xue, Z.-Q. Yin, S. Jia, and L. Sun, Phys. Rev. Lett. **123**, 080501 (2019).
[33] F. Pirmoradian, B. Z. Rameshti, M. Miri, and S. Saeidian, Phys. Rev. B **98**, 224409 (2018).
[34] K. Yu. Guslienko, B. A. Ivanov, V. Novosad, Y. Otani, H. Shima, and K. Fukamichi, J. Appl. Phys. **91**, 8037 (2002).
[35] M. Mochizuki, Phys. Rev. Lett. **108**, 017601 (2012).
[36] Y. Onose, Y. Okamura, S. Seki, S. Ishiwata, and Y. Tokura, Phys. Rev. Lett. **109**, 037603 (2012).
[37] J. Shibata, K. Shigeto, and Y. Otani, Phys. Rev. B **67**, 224404 (2003).
[38] J. Shibata and Y. Otani, Phys. Rev. B **70**, 012404 (2004).
[39] D.-S. Han, A. Vogel, H. Jung, K.-S. Lee, M. Weigand, H. Stoll, G. Schutz, P. Fischer, G. Meier, and S.-K. Kim, Sci. Rep. **3**, 2262 (2013); J. Kim, J. Yang, Y.-J. Cho, B. Kim, and S.-K. Kim, *ibid.* **7**, 45185 (2017).
[40] A. Barman, S. Barman, T. Kimura, Y. Fukuma, and Y. Otani, J. Phys. D **43**, 422001 (2010); S. Barman, A. Barman, and Y. Otani, IEEE Trans. Magn. **46**, 1342 (2010).
[41] A. Vogel, A. Drews, T. Kamionka, M. Bolte, and G. Meier, Phys. Rev. Lett. **105**, 037201 (2010).
[42] S. Sugimoto, Y. Fukuma, S. Kasai, T. Kimura, A. Barman, and Y. Otani, Phys. Rev. Lett. **106**, 197203 (2011).
[43] T. Taniuchi, M. Oshima, H. Akinaga, and K. Ono, J. Appl. Phys. **97**, 10J904 (2005); B. C. Choi, J. Rudge, E. Girgis, J. Kolthammer, Y. K. Hong, and A. Lyle, Appl. Phys. Lett. **91**, 022501 (2007); Y.-S. Choi, M.-W. Yoo, K.-S. Lee, Y.-S. Yu, H. Jung, and S.-K. Kim, *ibid.* **96**, 072507 (2010).
[44] Z.-X. Li, Y. Cao, P. Yan, and X. R. Wang, npj Comput. Mater. **5**, 107 (2019).
[45] Z.-X. Li, Y. Cao, X. R. Wang, and P. Yan, arXiv:1910.03956.
[46] A. A. Thiele, Phys. Rev. Lett. **30**, 230 (1973).
[47] J. Zak, Phys. Rev. Lett. **62**, 2747 (1989).
[48] N. Wu, Phys. Lett. A **376**, 3530 (2012).
[49] G. Go, K. T. Kang, and J. H. Han, Phys. Rev. B **88**, 245124 (2013).
[50] G. de. Loubens, Phys. Rev. Lett. **102**, 177602 (2009).
[51] A. E. Ekomasov, S. V. Stepanov, K. A. Zvezdin, and E. G. Ekomasov, Phys. Met. Metallogr. **118**, 328 (2017).
[52] T. Maruyama, Y. Shiota, T. Nozaki, K. Ohta, N. Toda, M. Mizuguchi, A. A. Tulapurkar, T. Shinjo, M. Shiraishi, S. Mizukami, Y. Ando, and Y. Suzuki, Nat. Nanotechnol. **4**, 158 (2009).